The crystalline lattice of URu_2Si_2 under pressure in the paramagnetic, hidden order, and antiferromagnetic states

J. R. Jeffries,[1] N. P. Butch,[2] J. J. Hamlin,[3] S. V. Sinogeikin,[4] W. J. Evans,[1] and M. B. Maple[3]

[1] *Condensed Matter and Materials Division, Lawrence Livermore National Laboratory, Livermore, CA 94550, USA*
[2] *Center for Nanophysics and Advanced Materials, Department of Physics, University of Maryland, College Park, MD 20742, USA*
[3] *Department of Physics, University of California, San Diego, La Jolla, CA 92093, USA*
[4] *HPCAT, Advanced Photon Source, Argonne National Laboratory, Argonne, IL 60439, USA*

(Dated: February 14, 2022)

X-ray diffraction experiments under pressure in a diamond anvil cell have been performed to gauge any response of the crystalline lattice of URu_2Si_2 to the "hidden order" or antiferromagnetic transitions, the latter of which is accessible only with applied pressure. The ambient-pressure crystal structure of URu_2Si_2 persists to high pressure, and structural characterization reveals a reasonably robust crystal lattice with respect to *both* of the aforementioned temperature-induced electronic transitions. Coupling between the lattice and the "hidden order" transition is reconfirmed to be subtle, and that subtle sensitivity is extended to the antiferromagnetic transition. The pressure-dependent evolution of the lattice parameters indicates a slightly anisotropic compression of the unit cell, which results in a decrease in the lattice c/a ratio with increasing pressure. From compression data, the bulk modulus is estimated to be $B_0 \approx$190 GPa. While the unit cell volume undergoes compression, the Ru-Si layers separating the U planes evince an apparent "flattening," resulting in a more 2D-like structure and an increased volume per U ion.

PACS numbers: 71.27.+a, 64.70.kd, 61.05.cp

I. INTRODUCTION

The moderately heavy fermion compound URu_2Si_2 has inspired numerous experimental and theoretical studies associated with the "hidden order" (HO) transition at T_0=17.5 K.[1–3] Despite over two decades of study, the nature of the order parameter of the HO phase of URu_2Si_2 remains one of the persistent mysteries of strongly correlated condensed-matter systems. The HO transition is revealed as an anomaly in nearly every bulk measurement; but, the antiferromagnetic sublattice magnetization at the commensurate wavevector Q_c=(1,0,0) is insufficient to account for the entropy released during the transition.[4,5] The small, commensurate moment in the HO phase is now generally regarded as a non-intrinsic, parasitic quality of URu_2Si_2, perhaps engendered by pressure inhomogeneities or impurity-derived strains.[6,7] Below T_0, the development of additional gapped spin excitations centered at an incommensurate wavevector Q_i=(1.4,0,0) can, however, account for the entropy reduction associated with the onset of the HO phase.[8] An energy gap at the Fermi surface opens at temperatures below the HO transition, but that gap is incomplete, leaving residual density of states for metallic conduction and the eventual onset of superconductivy.[3] Surprisingly, the antiferromagnetic fluctuations of the HO phase can be suppressed with small Re doping, which quickly gives rise to ferromagnetic fluctuations and criticality, the repercussions of which are not fully understood.[9]

Under pressure, the HO transition temperature increases and evinces a kink in its pressure dependence at a critical pressure P_c=15 kbar,[10–12] by which point the partial Fermi surface gap of the HO state has grown to consume an entire portion of the Fermi surface, destroying superconductivity.[13] Above P_c, neutron diffraction and ^{29}Si NMR measurements establish a large moment antiferromagnetic (AFM) phase as the ground state of the system.[14–16] The HO phase yields to this high-pressure AFM phase via a first-order transition line that extrapolates to zero temperature near $P_x \approx$7 kbar.[16–19] The position of this first-order HO/AFM transition in the pressure-temperature phase diagram is somewhat controversial, and may be affected by pressure-induced strains in non-hydrostatic pressure-transmitting media.[20] Recent theoretical predictions suggest a strong coupling between or unification of the order parameters of the HO and AFM states,[21] with some calculations advocating near energetic degeneracy between the two phases.[22] The details of the HO/AFM coupling and how it engenders the phase diagram of URu_2Si_2, including the disappearance of superconductivity, are important questions concerning the nature of the HO phase. Nesting of the Fermi surface, either incommensurate or commensurate, seems to be a common feature of both the HO and AFM states, but there are discrepancies between calculated and experimentally obtained Fermi surfaces.[22–24] Magnetic contributions from the *f*-electrons, multipoles, and crystalline electric fields from the crystalline lattice have been proposed as mechanisms responsible for the ordering of URu_2Si_2.[24–28]

At ambient pressure, and persisting down to 4.2 K, URu_2Si_2 crystallizes in the tetragonal $ThCr_2Si_2$ crystal structure (space group 139, I4/mmm) with lattice parameters a=4.1239 Å and c=9.5817 Å.[1] The tetragonal lattice manifests anisotropies in bulk properties such as magnetic susceptibility, resistivity, and

thermal conductivity.[1,12,29–32] At the HO transition, there is a large increase in the thermal conductivity, with the increase being largely dominated by phonon conduction.[33,34] Thermal conductivity, specific heat, and point-contact-spectroscopy measurements have been used to infer strong coupling between the order parameter of the HO state and the crystalline lattice.[34,35] Measurements of elastic constants suggest that there is no uniform lattice distortion associated with the onset of the HO state, but those same measurements do suggest a lattice softening below 70 K,[36] near the coherence temperature as determined from electrical resistivity measurements. Dilatometry experiments reveal that the HO transition induces a contraction of the a lattice parameter and an expansion of the c lattice parameter.[17,37,38] Under pressure, additional thermal expansion signatures, corresponding to the onset of the large moment AFM phase, develop along both the a- and c-axes. These new AFM signatures are in the same direction as the signatures of the HO transition (*i.e.*, contraction along a and expansion along c), but they are significantly larger in magnitude.[17] Currently, it is not known how the microscopic crystalline lattice distorts to accommodate these observed length changes.

Lattice coupling, Fermi surface gapping, and the presence of spin excitations collude to imply a spin density wave (SDW) scenario as a possible description of the HO state. Previous ambient-pressure experiments suggest that the HO transition does not alter the symmetry of the crystalline lattice;[39] however, a detailed picture of the evolution of the crystal structure with *both* temperature and pressure has not been advanced. In this paper, we report the results of a high-pressure x-ray diffraction study examining the lattice response of URu_2Si_2 to pressure and temperature, with a specific focus on any correlations between lattice stability and the onset of either HO or AFM.

II. EXPERIMENTAL DETAILS

A single crystal of URu_2Si_2 was grown via the Czochralski technique in a tetra-arc furnace with an argon atmosphere. The crystal was annealed at 900 °C with a Zr getter in a partial pressure of argon for 7 days. The sample was confirmed to be a single crystal with the Laue method as well as electron diffraction. A portion of the single crystal was ground into a fine powder (<15 μm) to be used in the high-pressure diamond anvil cell (DAC) x-ray diffraction experiments.

Two Livermore-designed, membrane-driven DACs were used in this study. The DACs were fitted with matching pairs of 500 and 700 μm flat diamonds. Brass gaskets (250-μm thick) were pre-indented to thicknesses of 60-70 μm, after which, 350-μm sample chambers were drilled through the center of the indentation with an electric discharge machine. For contamination control purposes, Mylar and Kapton windows, which both exhibit low attenuation of x-rays, were affixed to the outside of the cell.

The powdered sample was loaded into the sample chambers of each DAC along with several micron-sized ruby and Sm-doped SrB_4O_7 chips for initial pressure calibration.[40,41] Liquid argon was loaded into the sample chamber cryogenically to serves as a nearly hydrostatic pressure-transmitting medium. Measurements were performed at three different pressures: 4 and 27 kbar in one DAC and 8 kbar in another. When the samples were cooled, these pressures probed different regions of the phase diagram corresponding to the PM/HO (4 kbar), the PM/HO/AFM (8 kbar), and PM/AFM (27 kbar) transitions. The DACs were pressurized at room temperature, and the pressure was measured *in situ* with an online ruby fluorescence setup using the pressure- and temperature-dependent position of the ruby R1 line.[40,42] Pressure gradients within the sample chamber remained below 1 kbar as measured by several distinct ruby chips in different regions of the sample chamber.

For temperature-dependent measurements, the DACs were seated in a liquid helium flow cryostat equipped with Kapton windows. The temperature was monitored with a silicon diode and controlled with a Lakeshore Model 340 temperature controller. With the heat load of the DAC and radiation through the translucent windows, a base temperature of about 6 K was achieved. A copper braid was attached to both the thermometer and the gasket of each DAC in order to ensure good thermal contact between the two.

Angle-dispersive X-ray diffraction (ADXD) experiments were performed at the HPCAT beamline 16 ID-B of the Advanced Photon Source at Argonne National Laboratory. A 5x10 μm, 33.6 keV (λ_{inc}=0.3694 Å) incident x-ray beam, calibrated with CeO_2, was used. This energy allowed for acceptable x-ray attenuation and increased the number of Bragg reflections present in the accessible 2Θ range. The experiments were performed in a transmission geometry with the incident beam entering through the table of one of the anvils and the diffracted signal exiting through the table of the opposing anvil. A slit in the DAC permitted the acquisition of the diffracted signal out to $2\Theta \approx 25°$. The diffracted x-rays were detected with a Mar345 image plate; exposure times ranged from 30-120 seconds. In order to achieve a good powder pattern, the incident beam was rastered (in actuality, the sample was moved while the beam was fixed) over a square area of the sample ranging from 30-100 μm on a side. 2D diffraction patterns were collapsed to 1D intensity versus 2Θ plots using the program FIT2D.[43] Pressure- and temperature-dependent lattice parameters were extracted by indexing the positions of the Bragg reflections using the programs GSAS[44,45] and XRDA;[46] both programs returned identical results within error.

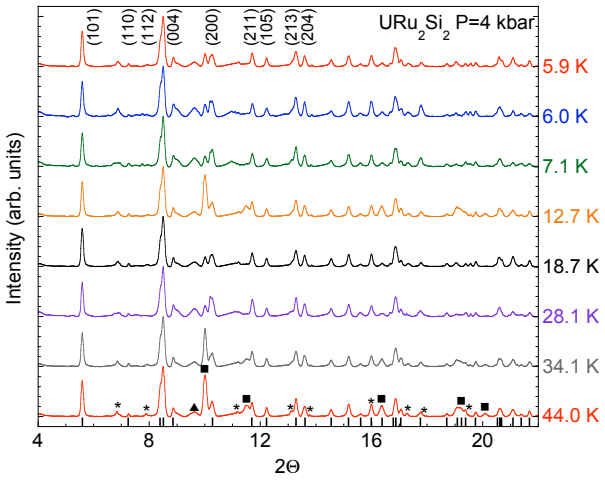

FIG. 1: (color online) ADXD patterns, intensity vs. 2Θ, of URu_2Si_2 at 4 kbar for various temperatures. In addition to being shifted vertically for clarity, the intensity of each diffraction pattern has been normalized relative to the maximum intensity of the (112) Bragg reflection near 2Θ ≈8.5°. Indicated to the right of each diffraction pattern are the temperatures at which each pattern was obtained. The position of the prominent Bragg reflections due to URu_2Si_2 are indicated as black vertical lines distributed along the abscissa, while selected Bragg peaks are marked on the topmost diffraction pattern. The bottom-most diffraction pattern is labeled with squares (■) to denote diffraction from the brass gasket, asteriks (∗) to denote diffraction from the solid argon pressure-transmitting medium, and triangles (▲) to denote diffraction from the Sm-doped SrB_4O_7 pressure marker.

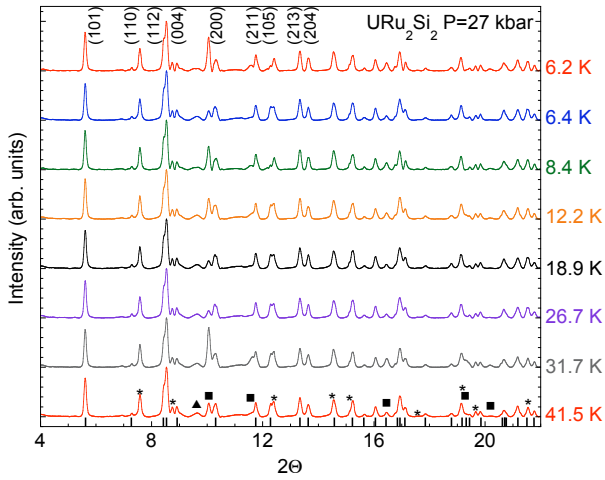

FIG. 2: (color online) Representative ADXD patterns of URu_2Si_2 at 27 kbar for various temperatures. Labeling, scaling, and vertical shifting conventions are the same as those of Fig. 1.

III. RESULTS

A. Crystal structure and symmetry

Figures 1 and 2 display representative, collapsed ADXD patterns (intensity versus 2Θ) of URu_2Si_2 at 4 and 27 kbar for various temperatures. The intensity of each diffraction pattern has been normalized to the intensity of the (112) Bragg peak and shifted vertically for clarity. The prominent Bragg reflections for URu_2Si_2—with lattice parameters a =4.1252 Å and c =9.5578 Å at 4 kbar and a =4.1093 Å and c =9.5152 Å at 27 kbar—are indicated as vertical black lines along the horizontal axes of Figures 1 and 2. Along the topmost diffraction pattern, several Bragg reflections are specified by the Miller indices of the planes satisfying the diffraction condition. It should be noted that the peak labeled as (112) is actually a double peak, which includes the (103) and (112) reflections that are not distinctly resolved at the incident energy used in the experiments. The angular separation of these two reflections at 33.6 keV is expected to be only 0.11°, approximately equal to the characteristic width (full width at half maximum) of most of the peaks.

In addition to the powdered sample, diffraction patterns from the brass gasket, argon pressure-transmitting medium, and Sm-doped SrB_4O_7 pressure markers are present; these non-sample contributions to the diffraction pattern are denoted in Figures 1 and 2 by squares, asteriks, and triangles (see figure captions). The peak positions of these non-sample contributions change little with temperature; however, the corresponding relative intensity varies depending on the volume of these non-sample contributions relative to the sample as slightly different regions of the DAC sample chamber are probed during rastering. All of the peaks in the diffraction patterns of Figures 1 and 2 can be indexed to URu_2Si_2, the gasket, the pressure-transmitting medium, and the pressure markers; no impurity phases associated with the sample are detected.

Measurements at a third, intermediate pressure of 8 kbar were performed in a second cell. In this DAC, significantly less sample was present within the sample chamber than the DAC from which the data in Figures 1 and 2 were obtained. The smaller amount of sample caused the sample to contribute significantly less to the total diffraction pattern than the brass gasket. The raw 8-kbar data are not displayed; however, the evolution of the data is intermediate between Figures 1 and 2 and of sufficient quality to extract much of the same information.

Figure 3 shows the ADXD patterns taken near 6 K, approximately the base temperature of the cryostat, for each pressure: 4, 8, and 27 kbar. In the 8-kbar diffraction pattern, any intensities greater than that of the URu_2Si_2 (112) peak have been truncated to fit on the same scale as the data from the other pressures. The two broad, truncated peaks in the 8-kbar data are from the brass gasket, which unfortunately obscure some of the Bragg reflections from the sample. With pressure, the URu_2Si_2

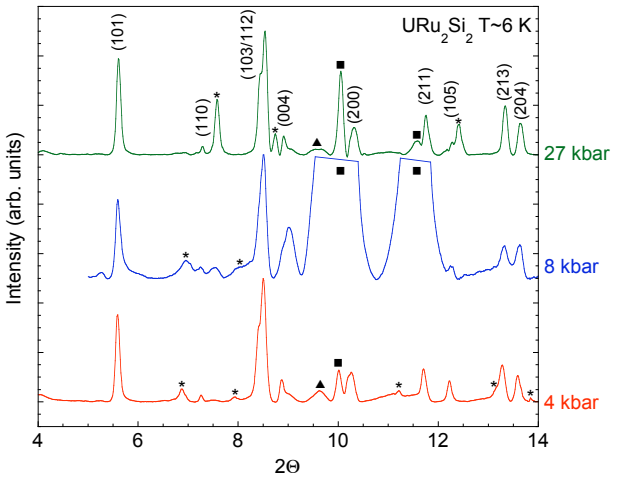

FIG. 3: (color online) Representative ADXD patterns of URu_2Si_2 near 6 K for each pressure measured. Labeling, scaling, and vertical shifting follow the conventions of Fig. 1. The data at 8 kbar have been truncated such that any intensity above that of the URu_2Si_2 (112) reflection is ignored. The broad, truncated peaks correspond to the brass gasket.

sample is compressed slightly, as evinced by the slight rightward shift in 2Θ of the Bragg peaks.

From Figures 1-3, it can be seen that there are no dramatic changes in the diffraction patterns with respect to temperature or pressure. Above and below the PM/HO and PM/AFM transition temperatures, the relative spacings of the Bragg reflections remain constant within the angular resolution afforded by the energy of the incident x-ray beam. Furthermore, no new peaks appear upon cooling through the PM/HO or PM/AFM transitions, which would occur below T_0(4 kbar)≈18 K and T_0(27 kbar)≈22 K. The pressure-dependent evolution of the crystal structure lacks any evidence of additional peaks or peaks that do not index with the URu_2Si_2 crystal structure. These facts suggest that the ambient-pressure lattice symmetry and crystal structure persist in the PM, HO, and AFM phases.

B. Temperature- and pressure-dependent lattice constants

The lattice parameters were calculated from the diffraction patterns obtained at different pressures and temperatures. The results of these calculations are shown in Figure 4, where a, c, and the unit cell volume v are plotted as a function of temperature for each pressure measured. The error bars are returned from structural analysis.

At all pressures, the c lattice parameter shows a gentle expansion, while the a lattice parameter and the unit cell volume exhibit roughly constant values as a function of temperature. At 4 and 8 kbar, the a lattice parameter, and consequently the unit cell volume, may exhibit contraction below 20 K. While this potential contraction along the a-axis is qualitatively consistent with previous dilation experiments at low temperature and under pressure,[17,37] the magnitude of the uncertainty in lattice parameters forbids a definitive claim of such contraction (*i.e.*, a horizontal line fits within the error bars of each point). At about 4 kbar and from the PM/HO transition down to 10 K, Motoyama *et al.* found a contraction parallel to the a-axis of roughly 4 parts in 10^{-5} and an expansion along the c-axis of less than 1 part in 10^{-5}.[17] On the contrary, at about 16 kbar and from the PM/AFM transition down to 10 K, they found a contraction parallel to the a-axis of 7 parts in 10^{-5} and an expansion along the c-axis of about 5 parts in 10^{-5}. Recent Larmor diffraction experiments show similar results.[47] The arrows in Figure 4 represent the approximate temperatures where the PM/HO or PM/AFM transitions should occur. There is no evidence of any discontinuity in the temperature dependence of the lattice parameters near these

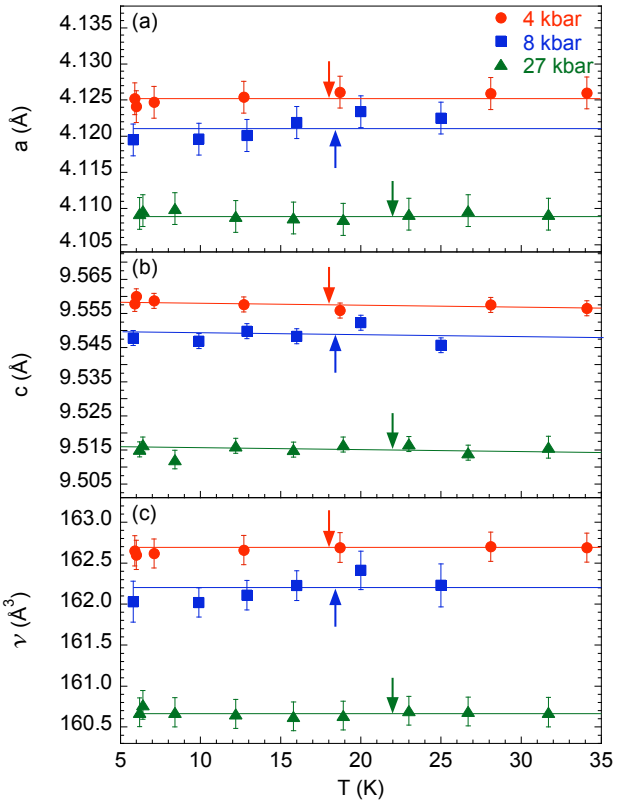

FIG. 4: (color online) Temperature-dependent lattice parameters a (a), c (b), and unit cell volume v (c) of URu_2Si_2 determined for different pressures. The arrows indicate the approximate positions of the PM/HO and PM/AFM transition temperatures.[13] The solid lines are guides to the eye. Error bars are described in the text.

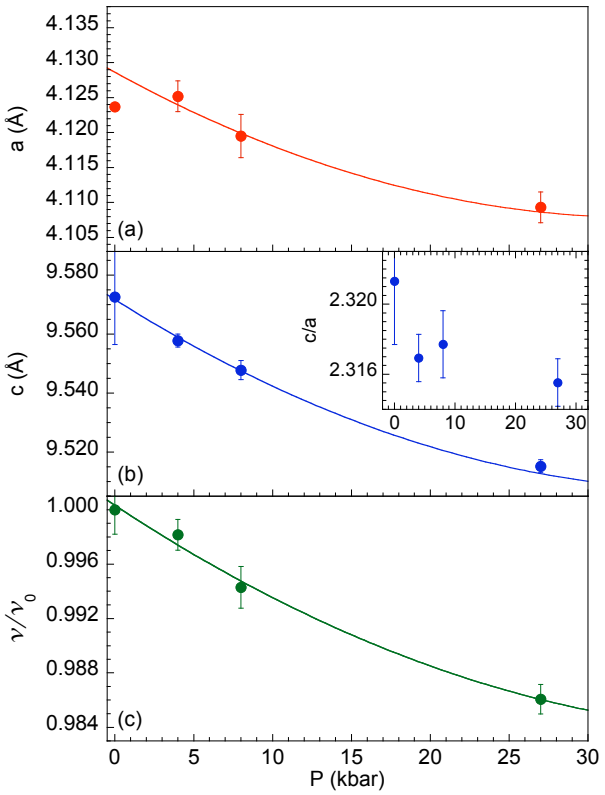

FIG. 5: (color online) Lattice parameters a (a) and c (b) as well as the relative unit cell volume v/v_0 (c) at 6 K as a function of pressure. The solid lines are guides to the eye. Error bars are described in the text. The inset of (b) shows the pressure-dependent c/a ratio versus pressure. The zero-pressure data points and their error bars represent, respectively, averages and standard deviations of previously reported low-temperature lattice parameters.[29,48,49]

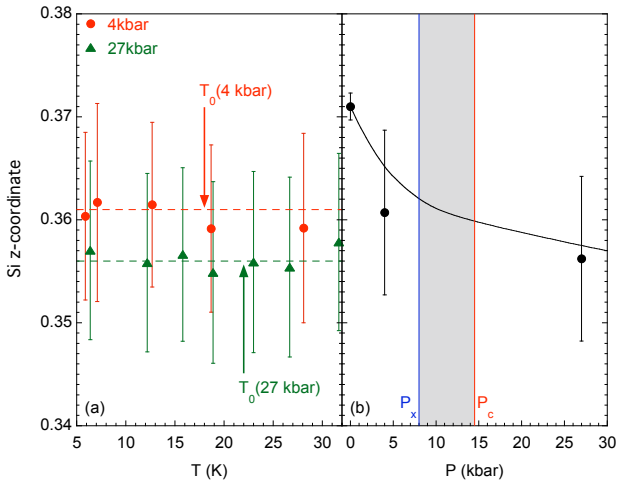

FIG. 6: (color online) (a) The Si z-coordinate within the lattice as a function of T for P=4 and 27 kbar. The horizontal, dashed line represent the mean values of z for each pressure, and the HO or AFM transitions are denoted by the arrows. Entering the HO or AFM states does not largely affect the positions of the Si atoms. (b) The evolution of z as a function of P at T=6 K. The vertical blue line represents the pressure P_x where the HO state yields to antiferromagnetism at low temperature, the vertical red line represents the critical pressure P_c where T_0 exhibits a kink in its pressure dependence, and the grey swath represents the pressure range over which P_x evolves toward P_c with increasing temperature and pressure. The solid line is a guide to the eye. Error bars are returned from structural refinement.

phase transitions; however, while the length changes from dilatometry measurements indicate a different lattice response to the onset of HO or AFM, it should be noted that those length changes are at least two orders magnitude below the resolution of our experiment.

The lattice parameters, a and c, and the relative unit cell volume—v/v_0, with v_0 =162.95 Å^3 being the ambient pressure unit cell volume—at 6 K are displayed as a function of pressure in Figure 5. The zero-pressure values of the lattice parameters are taken from the literature.[29,48,49] With applied pressure, both lattice parameters decrease, with a and c decreasing by approximately 0.4% and 0.7%, respectively, by 27 kbar. This slight anisotropic contraction of URu_2Si_2 under pressure is demonstrated by the slight reduction in the c/a ratio (inset of Fig. 5) with increasing pressure. Although more data points would be ideal for such a conclusion, the data point at 8 kbar may suggest a discontinuity in the evolution of the c/a ratio, which could be a consequence of crossing the HO/AFM phase boundary. The decrease in the unit cell along the a- and c-axes manifests a 1.4% contraction of the unit cell volume by 27 kbar, consistent with previous x-ray diffraction measurements.[48] The low-pressure slope of Fig. 5(c) indicates a bulk modulus B_0≈190 GPa, smaller than the room-temperature estimate of Luo *et al.*[50], but in excellent agreement with that reported by Kuwahara *et al.*[48]

C. Si lattice sites

Within the $ThCr_2Si_2$ crystal structure, the Si atoms occupy sites (Wyckoff position 4e) with a free z-parameter in the lattice coordinates. The Si atoms of URu_2Si_2 can thus shift vertically within the unit cell without altering the crystal structure or symmetry defining the positions of the Bragg reflections. Any changes in this z-coordinate instead manifest as changes in the relative intensity of the Bragg reflections. Structural refinement of the intensities thus yields information about the position of the Si atoms within the crystalline lattice. For the case of URu_2Si_2 at ambient pressure, this z-coordinate is reported to be z =0.3710±0.0013.[51]

The positions of the Si atoms within the URu_2Si_2 crys-

tal structure are shown in Figure 6 as a function of temperature (a) and pressure (b). The prominent diffraction of the brass gasket in the 8-kbar data obscures several Bragg peaks from URu_2Si_2 and prevents a robust analysis of the Bragg peak intensities at that pressure. The combination of a small number of powdered crystallites in the DAC as well as the tendency for URu_2Si_2 to cleave in the basal plane may induce a texturing effect (*i.e.,* a preferred orientation of the powdered sample) in the powder diffraction patterns. This texturing would skew the relative intensities of the Bragg peaks depending on the specific preferred orientation, introducing greater uncertainty into the determination of z for the Si site.

The z-coordinate changes little with temperature for both pressures where the analysis could be performed. The mean values of z at 4 and 27 kbar are 0.3609 and 0.3562, respectively (shown as horizontal, dashed lines in Fig. 6a). For both pressures, the calculated values stay within approximately 0.2% of those means from 6 - 30 K. At approximately 2%, the uncertainties (error bars in Fig. 6a) in the determination of z are an order of magnitude larger than the standard deviation over the above temperature range and about 6 times larger than the uncertainty in the ambient-pressure value of z.[51] From these data, it would seem that the positions of the Si atoms in the lattice are not strongly affected by the onset of the HO or AFM states. With increasing pressure (Fig. 6b), the value of z at 6 K decreases. This change in the z coordinate of the Si site results in a "flattening" of the Ru-Si cage surrounding the U ions (see Figure 7) and significant changes in specific bond lengths (see Table I).

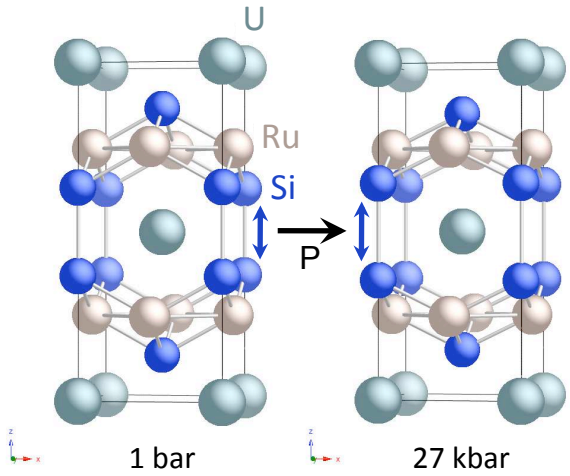

FIG. 7: (color online) The crystal structures of URu_2Si_2 at ambient pressure and 27 kbar. Bonding in the Ru-Si layers is shown to emphasize the shift in the positions of the Si atoms. Despite compression of the unit cell volume and shrinking of the c-axis with pressure (both of which are included in the 27-kbar structure), the Ru-Si layer flattens, *increasing* the Si-Si interlayer bond length (highlighted by the double-headed, vertical arrows) and the U-Si first nearest neighbor bond length.

IV. DISCUSSION

In the HO state of URu_2Si_2, strong coupling to the lattice has been proposed on the grounds of thermal conductivity experiments.[34] A spin- or charge-density wave is a natural scenario where charge degrees of freedom undergo a modulation, and that modulation can couple to the lattice.[52,53] The degree of that coupling and its effects on observable parameters of the lattice, however, are dependent upon details of the density wave. In the case of the static, commensurate charge-density-wave (CDW) in α-U (the only example of a CDW in an element), superlattice reflections appear in diffraction and the atoms along a are displaced by about 0.03 Å from their equilibrium positions at temperatures above the CDW transition (the displacements are different along different crystallographic axes, with the a-axis showing the largest displacement).[54] Consistently, specific heat measurements of single-crystal α-U conclude a similar strong lattice coupling of the low-temperature α_3 CDW phase.[55] The entropy released during this α_3 transition is ΔS_{α_3}=0.05 J/mol-K, more than 20 times less than the entropy released during the HO transition in URu_2Si_2; an energy gap for the α_3 transition was not extracted from the specific heat of α-U. The inorganic dichalcogenide 2H-$TaSe_2$ displays commensurate CDW ordering below 90 K, below which temperature a gap at the Fermi surface opens and approaches 60 meV at zero temperature.[56] The atomic displacements of the lattice associated with the CDW in 2H-$TaSe_2$ are as large as 0.05 Å.[57] When compared with 2H-$TaSe_2$, URu_2Si_2 has a more modest Fermi surface gapping at the HO transition of 11 meV[3] and, from these experiments, no observable lattice displacements.

For the case of URu_2Si_2 at ambient pressure, spin fluctuations have been observed in the HO state, but those spin fluctuations are both dynamic and incommensurate. The gapping of these spin fluctuations may be able to account for the entropy released during the HO transition,[8] but the ordering that controls their presence is not fully understood, and whether a density wave is responsible for the order parameter of the HO state remains an open question. The absence of any strong superlattice reflections or significant atomic displacements in the diffraction data at 4 kbar does not implicate a density wave as the mechanism for ordering. At high pressures, where the HO state gives way to a large-moment AFM state, static order develops along a commensurate (100) wavevector below the PM/AFM transition.[16] From the ADXD patterns at 27 kbar, there is no evidence in the form of strong superlattice reflections or atomic displacements that would suggest a "strong" coupling of the lattice to

TABLE I: Selected bond lengths of URu_2Si_2 near 6 K. The pressure-induced change in the Si z-coordinate manifests changes in bond lengths in addition to those expected from lattice contraction alone. First and second nearest neighbor bonds are denoted as 1^{st} NN and 2^{nd} NN, respectively. A positive (negative) change in bond length, Δ_{bl}, indicates an increase (decrease) in bond length.

	1 bar	27 kbar	Δ_{bl}(%)
Lattice parameters:			
a (Å)	4.128[a]	4.109	
c (Å)	9.578[a]	9.515	
Si z-coordinate	0.371[b]	0.356	
Bond lengths (Å):			
Ru-Ru	2.919[a]	2.906	-0.4
U-Ru	3.161[a]	3.143	-0.6
Ru-Si	2.367[a]	2.289	-3.3
Si-Si 1^{st} NN	2.471[a]	2.737	10.7
Si-Si 2^{nd} NN	3.727[a]	3.539	-5.0
U-Si 1^{st} NN	3.170[a]	3.211	1.3
U-Si 2^{nd} NN	3.553[a]	3.389	-4.6

[a]taken or calculated from Palstra *et al.*[1]
[b]from Cordier *et al.*[51]

this AFM state. It would seem that the lattice is coupled only subtly to the onset of both the HO and AFM states.

While the temperature dependence of the lattice is relatively unchanging, the lattice structure does evolve with pressure. Under pressure, the c/a ratio decreases, the unit cell volume decreases, the Si atoms shift position, and the bond lengths are altered between ambient pressure and 27 kbar (Table I). The compression of the unit cell volume is solely responsible for the modest shortening (around 0.5% for nearest neighbors) of the bonds not including Si atoms. The change in the Si z-coordinate, however, has significant impact on the bond lengths of the Si-inclusive bonds at 27 kbar: the Ru-Si bond length decreases by more than 3%, the Si-Si first nearest neighbor bond length (the bond directed along the c-axis between the Ru-Si layers) *increases* by more than 10%, the second nearest neighbor Si-Si bond length (the intralayer bond directed from the unit cell edge toward the central Si site on the opposite side of the Ru layer) decreases by 5%, the U-Si first nearest neighbor bond length (the U-Si bond directed from the center toward the Si atoms on the edge of the unit cell) *increases* by more than 1%, and the second nearest neighbor U-Si bond length (the U-Si bond directed along the c-axis of the unit cell) decreases by over 4%.

These changes in bond lengths may have significant ramifications for the development of the low-temperature ordered phases. The contraction of the Ru-Si bond length compresses the Ru-Si layers vertically, while the large change in the Si-Si first nearest neighbor bond likely results in decreased bonding between opposing Ru-Si layers. These two facts conspire to create a more 2D-like lattice structure with corrugated Ru-Si layers separating U planes. This reduction in coupling of Ru-Si layers may have dramatic consequences on the Fermi surface and the location of gaps and nesting vectors within it, including the pressure-induced development of the large-moment AFM phase at Q_c=(1,0,0). The compression-induced change in the U-Ru bond and the opposing changes in the first and second nearest neighbor U-Si bonds have the effect of decreasing the anisotropy of U bonding. Additionally, the combination of bond length changes at high pressure effectively induces a larger volume per U ion within the crystalline lattice. The decrease in the anisotropy of bonding and the effective volume per U ion may have important consequences to the degree of f-electron hybridization and the development of AFM order.

Several recent theoretical descriptions of the ground states of URu_2Si_2 espouse subtle variations in the Fermi surface as the contributors to the disparate HO and AFM states.[22,24] It is possible that the observed slight pressure-induced lattice variations are sufficient to alter the nesting vectors of the Fermi surface, the f-electron contributions, or the crystalline electric field environment, thus affecting the ground state of the system. The degree to which the change in lattice environment may affect the electronic ordering will require more study, but may be a fruitful path forward in explaining the disparities and similarities of the HO and AFM states.

V. CONCLUSIONS

We have investigated the crystal structure of URu_2Si_2 as a function of pressure and temperature, with a particular focus on any lattice response to the onset of the HO or AFM states. From these experiments, we conclude that there are no dramatic consequences to the stability of the crystalline lattice with respect to either the PM/HO or PM/AFM transitions. X-ray diffraction patterns reveal that the ambient-pressure $ThCr_2Si_2$ structure persists to high pressures. In addition, there is no evidence in favor of the appearance of additional peaks with pressure or temperature, meaning that the lattice symmetry or structure remains unaltered with either the PM/HO transition at low pressure or the PM/AFM transition at elevated pressure. No strong superlattice reflections, as may be seen in a CDW or SDW, were observed. The lattice parameters were calculated from the positions of the Bragg reflections of URu_2Si_2, and there is no evidence that the HO or AFM states induce a large scale, uniform change ($\gtrsim$ 1 part in 1000) in lattice constants relative to the PM state. Furthermore, the relatively constant intensities of the Bragg reflections with respect to temperature at a given pressure indicate that the Si atoms likely remain within less than 2% of their original positions with the onset of either the HO or AFM states.

Any coupling of the HO or AFM order parameters to the crystalline lattice must result in only subtle variations of the parent PM phase.

With increasing pressure, the a- and c-axes of the unit cell both contract, with the c-axis contracting slightly more than the a-axis. This anistropic contraction results in a slight reduction in the c/a ratio with increasing pressure, as well as an overall compression of the unit cell volume. The z-coordinate of the Si sites decreases with applied pressure. This has the effect of flattening the Ru-Si layers of the URu_2Si_2 crystal structure, which leads to a more 2D-like structure and a larger volume per U ion. These effects may have consequences to the f-electron hybridization and the Fermi surface of URu_2Si_2.

VI. ACKNOWLEDGMENTS

We are grateful to H. Cynn, B. J. Baer, Z. Jenei, and K. Visbeck for assistance with cell preparations and useful discussions. We also thank C. Kenny-Benson and E. Rod for beamline support. Sample synthesis was supported by the U.S. Department of Energy under Research Grant DE-FG-02-04ER46105. JRJ and WJE are supported by the Science Campaign at Lawrence Livermore National Laboratory. NPB is supported by the Center of Nanophysics and Advanced Materials. JJH and MBM are supported by the National Nuclear Security Administration under the Stewardship Science Academic Alliance program through the U.S. Department of Energy under Grant No. DE-FG52-06NA26205. Lawrence Livermore National Laboratory is operated by Lawrence Livermore National Security, LLC, for the U.S. Department of Energy, National Nuclear Security Administration under Contract DE-AC52-07NA27344. Portions of this work were performed at HPCAT (Sector 16), Advanced Photon Source (APS), Argonne National Laboratory. HPCAT is supported by DOE-BES, DOE-NNSA, NSF, and the W.M. Keck Foundation. APS is supported by DOE-BES, under Contract No. DE-AC02-06CH11357.

[1] T. T. M. Palstra,A. A. Menovsky, J. van den Berg, A. J. Dirkmaat,P. H. Kes, G. J. Nieuwenhuys and J. A. Mydosh, Phys. Rev. Lett **55**, 2727 (1985).
[2] W. Schlabitz, J. Baumann, B. Pollit, U. Rauchschwalbe, H. M. Mayer, U. Ahlheim, and C. D. Bredl, Z. Phys. B **62**, 171 (1986).
[3] M. B. Maple, J. W. Chen, Y. Dalichaouch, T. Kohara, C. Rossel, M. S. Torikachvili, M. W. McElfresh, and J. D. Thompson, Phys. Rev. Lett **56**, 185 (1986).
[4] C. Broholm, J. K. Kjems, W. J. L. Buyers, P. Matthews, T. T. M. Palstra, A. A. Menovsky, and J. A. Mydosh, Phys. Rev. Lett. **58**, 1467 (1987).
[5] C. Broholm, H. Lin, P. T. Matthews, T. E. Mason, W. J. L. Buyers, M. F. Collins, A. A. Menovsky, J. A. Mydosh, and J. K. Kjems, Phys. Rev. B **43**, 12809 (1991).
[6] H. Amitsuka, K. Matsuda, I. Kawasaki, K. Tenya, M. Yokoyama, C. Sekine, N. Tateiwa, T. S. Kobayashi, S. Kawarazaki, and H. Yoshizawa, J. Magn. Magn. Mater. **310**, 214 (2007).
[7] P. G. Niklowitz, C. Pfleiderer, T. Keller, M. Vojta, Y. -K. Huang, and J. A. Mydosh, arXiv:0909.2071v1 (unpublished).
[8] C. R. Weibe, J. A. Janik, G. J. MacDougall, G. M. Luke, J. D. Garrett, H. D. Zhou, Y. -J. Jo, L. Balicas, Y. Qiu, J. R. D. Copley, Z. Yamani, and W. J. L. Buyers, Nat. Phys. **3**, 96 (2007).
[9] N. P. Butch and M. B. Maple, Phys. Rev. Lett. **103**, 076404 (2009).
[10] M. W. McElfresh, J. D. Thompson, J. O. Willis, M. B. Maple, T. Kohara, and M. S. Torikachvili, Phys. Rev. B **35**, 43 (1987).
[11] J. P. Brison, P. Lejay, A. Buzdin, and J. Flouquet, Physica C **229**, 79 (1994).
[12] J. R. Jeffries, N. P. Butch, B. T. Yukich, and M. B. Maple, J. Phys.: Condens. Matter **20**, 095225 (2008).
[13] J. R. Jeffries, N. P. Butch, B. T. Yukich, and M. B. Maple, Phys. Rev. Lett. **99**, 217207 (2007).
[14] H. Amitsuka, M. Sato, N. Metoki, M. Yokoyama, K. Kuwahara, T. Sakakibara, H. Morimoto, S. Kawarazaki, Y. Miyako, and J. A. Mydosh, Phys. Rev. Lett. **83**, 5114 (1999).
[15] K. Matsuda, Y. Kohori, T. Kohara, H. Amitsuka, K. Kuwahara, and T. Matsumoto, J. Phys.: Condens. Matter **15**, 2363 (2003).
[16] F. Bourdarot, A. Bombardi, P. Burlet, M. Enderle, J. Flouquet, P. Lejay, N. Kernavanois, V. P. Mineev, L. Paolasini, M. E. Zhitomirsky, and B. Fåk, Physica B **359-361**, 986 (2005).
[17] G. Motoyama, T. Nishioka, and N. K. Sato, Phys. Rev. Lett. **90**, 166402 (2003).
[18] E. Hassinger, G. Knebel, K. Izawa, P. Lejay, B. Salce, and J. Flouquet, Phys. Rev. B **77**, 115117 (2008).
[19] A. Villaume, F. Bourdarot, E. Hassinger, S. Raymond, V. Taufour, D. Aoki, and J. Flouquet, Phys. Rev. B **78**, 012504 (2008).
[20] N. P. Butch, J. R. Jeffries, D. A. Zocco, and M. B. Maple, High Pressure Res. **29**, 335 (2009).
[21] V. P. Mineev and M. E. Zhitomirsky, Phys. Rev. B **72**, 014432 (2005).
[22] S. Elgazzar, J. Rusz, P. M. Oppeneer, and J. A. Mydosh, Nat. Mater. **8**, 337 (2009).
[23] J. D. Denlinger, G. -H. Gweon, J. W. Allen, C. G. Olson, M. B. Maple, J. L. Sarrao, P. E. Armstrong, Z. Fisk, and H. Yamagami, J. Electron Spectrosc. Relat. Phenom. **117**, 347 (2001).
[24] K. Haule and G. Kotliar, Nat. Phys. **5**, 796 (2009).
[25] P. Santini and G. Amoretti, Phys. Rev. Lett. **73**, 1027 (1994).
[26] A. Kiss and P. Fazekas, Phys. Rev. B **71**, 054415 (2005).
[27] F. Cricchio, F. Bultmark, O. Grånäs, and L. Nordström, Phys. Rev. Lett. **103**, 107202 (2009).
[28] J. A. Janik, H. D. Zhou, Y. -J. Jo, L. Balicas, G. J. MacDougall, G. M. Luke, J. D. Garrett, K. J. McClellan, E. D. Bauer, J. L. Sarrao, Y. Qiu, J. R. D. Copley, Z. Yamani,

W. J. L. Buyers, and C. R. Wiebe, J. Phys.: Condens. Matter **21**, 192202 (2009).
[29] T. T. M. Palstra, A. A. Menovsky, and J. A. Mydosh, Phys. Rev. B **33**, 6527 (1986).
[30] J. P. Brison, N. Keller, A Vernière, P. Lejay, L. Schmidt, A. Buzdin, J. Flouquet, S. R. Julian, and G. G. Lonzarich, Physica C **250**, 128 (1995).
[31] C. Pfleiderer, J. A. Mydosh, and M. Vojta, Phys. Rev. B **74**, 104412 (2006).
[32] Z. Zhu, E. Hassinger, Z. Xu, D. Aoki, J. Flouquet, and K. Behnia, Phys. Rev. B **80**, 172501 (2009).
[33] K. Behnia, R. Bel, Y. Kasahara, Y. Nakajima, H. Jin, H. Aubin, K. Izawa, Y. Matsuda, J. Flouquet, Y. Haga, Y. Ōnuki, and P. Lejay, Phys. Rev. Lett. **94**, 156405 (2005).
[34] P. A. Sharma, N. Harrison, M. Jaime, Y. S. Oh, K. H. Kim, C. D. Batista, H. Amitsuka, and J. A. Mydosh, Phys. Rev. Lett. **97**, 156401 (2006).
[35] J. G. Rodrigo, F. Guinea, S. Vieira, and F. G. Aliev, Phys. Rev. B **55**, 14318 (1997).
[36] K. Kuwahara, H. Amitsuka, T. Sakakibara, O. Suzuki, S. Nakamura, T. Goto, M. Mihalik, A. A. Menovsky, A. de Visser, and J. J. M. Franse, J. Phys. Soc. Japan **66**, 3251 (1997).
[37] M. A. Lopez de la Torre, R. Villar, S. Vieira, M. S. Torikachvili, and M. B. Maple, J. Alloy. Compd. **181**, 171 (1992).
[38] N. H. van Dijk, A. de Visser, J. J. M. Franse, and A. A. Menovsky, Phys. Rev. B **51**, 12665 (1995).
[39] N. Kernavanois, P. D. de Réotier, A. Yaouanc, J. -P. Sanchez, K. D. LiB, and P. Lejay, Physica B **259-261**, 648 (1999).
[40] H. K. Mao, J. Xu, and P. M. Bell, J. Geophys. Res. **91**, 4673 (1986).
[41] F. Datchi, R. LeToullec, and P. Loubeyre, J. Appl. Phys. **81**, 3333 (1997).
[42] W. L. Vos and J. A. Schouten, J. Appl. Phys. **69**, 6744 (1991).
[43] A. Hammersley, S. Svensson, M. Hanfland, A. Fitch, and D. Häusermann, High Press. Res. **14**, 235 (1996).
[44] A. C. Larson and R. B. Von Dreele, Los Alamos National Laboratory Report LAUR 86-748 (1994).
[45] B. H. Toby, J. Appl. Crystallogr. **34**, 210 (2001).
[46] S. Desgreniers and K. Lagarec, J. Appl. Crystallogr. **27**, 432 (1994).
[47] P. G. Niklowitz, C. Pfleiderer, S. Mühlbauer, P. Böni, T. Keller, P. Link, J. A. Wilson, M. Vojta, and J. A. Mydosh, Physica B **404**, 2955 (2009).
[48] K. Kuwahara, H. Sagayama, K. Iwasa, M. Kohgi, S. Miyazaki, J. Nozaki, J. Nogami, M. Yokoyama, H. Amitsuka, H. Nakao, and Y. Murakami, Acta Phys. Pol. B **34**, 4307 (2003).
[49] T. E. Mason, B. D. Gaulin, J. D. Garrett, Z. Tun, W. J. L. Buyers, and E. D. Isaacs, Phys. Rev. Lett. **65**, 3189 (1990).
[50] H. Luo, S. Dabos, U. Benedict, and J. C. Spirlet, J. Less-Common Met. **142**, L23 (1988).
[51] G. Cordier, E. Czech, H. Schäfer, and P. Woll, J. Less-Common Met. **110**, 327 (1985).
[52] G. Grüner, Rev. Mod. Phys. **60**, 1129 (1988).
[53] G. Grüner, Rev. Mod. Phys. **66**, 1 (1994).
[54] G. H. Lander, E. S. Fisher, and S. D. Bader, Adv. Phys. **43**, 1 (1994).
[55] J. C. Lashley, B. E. Lang, J. Boerio-Goates, B. F. Woodfield, G. M. Schmiedeshoff, E. C. Gay, C. C. McPheeters, D. J. Thoma, W. L. Hults, J. C. Cooley, R. J. Hanrahan, Jr., and J. L. Smith, Phys. Rev. B **63**, 224510 (2001).
[56] K. Rossnagel, E. Rotenberg, H. Koh, N. V. Smith, and L. Kipp, Phys. Rev. B **72**, 121103(R) (2005).
[57] D. E. Moncton, J. D. Axe, and F. J. DiSalvo, Phys. Rev. B **16**, 801 (1977).